

A coupled 1-D atmosphere and 3-D canopy radiative transfer model for canopy reflectance, light environment, and photosynthesis simulation in a heterogeneous landscape

Hideki Kobayashi*, Hironobu Iwabuchi

Frontier Research Center for Global Change (FRCGC), Japan Agency for Marine-Earth Science and Technology (JAMSTEC), Japan

Received 9 February 2007; received in revised form 21 April 2007; accepted 21 April 2007

Abstract

Detailed knowledge of light interactions between the atmosphere and vegetation, and within vegetation are of particular interest for terrestrial carbon cycle studies and optical remote sensing. This study describes a model for 3-D canopy radiative transfer that is directly coupled with an atmospheric radiative transfer model (Forest Light Environmental Simulator, FLIES). The model was developed based on the Monte Carlo ray-tracing method using some existing modeling frameworks. To integrate the canopy radiative transfer model with atmosphere, the same numerical method, sampling technique, and variance reduction technique were employed in both the atmospheric and the canopy modules. Farquhar's leaf photosynthesis model was combined to calculate the canopy level photosynthesis from the light environmental parameters obtained by the radiative transfer calculation. In order to document the quality of the coupled model, we first compared the atmospheric radiative transfer module to well known 1-D atmospheric radiative transfer models, and then evaluated the 3-D canopy radiative transfer module against a series of test cases provided by the RAMI On-line Model Checker (ROMC). We used the model to show the impact of atmospheric properties and 3-D canopy structure on the directionality of downward photosynthetically active radiation (PAR) at the top of canopy, the 3-D distribution of absorbed PAR (APAR), and overall canopy photosynthesis. The results indicate the importance to consider angular geometry of incident light at TOC and 3-D canopy structure.

© 2007 Elsevier Inc. All rights reserved.

Keywords: 3-D canopy radiative transfer; Canopy reflectance; Photosynthetically active radiation; Monte Carlo method

1. Introduction

Detailed information of light interactions between atmosphere and vegetation, and within vegetation are of particular interest for terrestrial carbon cycle studies and optical remote sensing. Recent studies have shown that changes in the atmospheric radiation regime due to aerosols and clouds affect canopy photosynthesis (e.g., Chameides et al., 1999; Cohan et al., 2002; Gu et al., 2003; Kobayashi et al., 2005; Nemani et al., 2003; Niyogi et al., 2004; Roderick et al., 2001). An

increase/decrease in canopy photosynthesis and its degree, however, largely depends on atmospheric conditions and canopy structure. A mechanistic understanding is necessary to generalize the effect of the radiation regime on canopy photosynthesis.

After the interaction of light with atmospheric particles such as aerosols and clouds, several types of change occur simultaneously in the incident photosynthetically active radiation (PAR) at the top of the canopy (TOC). When aerosols and clouds are induced in the atmosphere, the total PAR decreases and the fraction of diffuse PAR increases. The spectral composition of diffuse PAR also changes (Dye, 2004; Min, 2005). These changes can be partially or fully considered in existing atmospheric radiative transfer models for PAR estimation (Frouin et al., 1989; Eck & Dye, 1991; Gu et al., 2004; Kobayashi et al., 2004; Liang et al., 2006; Pinker & Laszlo, 1992; Van Laake & Sanchez-Azofeifa, 2004). However, due to their simplicity, these approaches do not take into account the angular variability of the incident diffuse PAR,

* Corresponding author. Ecosystem Change Research Program, Frontier Research Center for Global Change (FRCGC), Japan Agency for Marine-Earth Science and Technology (JAMSTEC), 3173-25, Showa-machi, Kanazawa-ku Yokohama, Kanagawa 236-0001, Japan. Tel.: +81 45 778 5666; fax: +81 45 778 5706.

E-mail address: hkoba@jamstec.go.jp (H. Kobayashi).

while incident diffuse light has directionality due to the strong forward scattering properties in aerosols and clouds. Also few measurements are available for incident PAR, including its angular variability. Therefore, canopy photosynthesis calculations tend to use the isotropic diffuse PAR in their absorbed PAR (APAR) and canopy photosynthesis calculations (e.g., Alton et al., 2005; De Pury & Farquhar, 1997; Guillevic & Gastellu-Etchegorry, 1999; Sellers, 1985, 1987; Sellers et al., 1992). This assumption regarding the radiation regime gives rise to APAR and photosynthesis errors of up to 15% in some cases (Grant, 1985; Wang & Jarvis, 1990).

In addition to the radiation regime in the atmosphere, the 3-D structure of the canopy makes the spatial light environment (reflectance, transmittance, and absorption) heterogeneous, especially for the forest canopy. Crown structure, leaf area density in the crown, tree density, and leaf/background optical properties affect 3-D variations in the light environment. At the fine resolution scale, light interactions in lateral directions are not negligible, being typically less than the Landsat spatial scale (<30 m; Widlowski et al., 2006).

Further understanding of light interactions (reflectance, transmittance, and absorption) between the atmosphere and the 3-D canopy should be achieved by theoretical consideration using detailed radiative transfer calculations. Physically based coupled atmosphere–canopy radiative transfer simulation enables the user to evaluate canopy photosynthesis under various atmospheric scenarios.

Several models exist for the calculation of 3-D canopy radiative transfer (e.g., Gastellu-Etchegorry et al., 1996; Govaerts & Verstraete, 1998; Myneni et al., 1991; North, 1996). Although 3-D canopy radiative transfer models may be linked to atmospheric radiative transfer models by the off-line simulation, which describes the angular distribution of atmosphere or canopy radiation at the atmosphere–canopy boundary via parametric interfaces (e.g. Widlowski et al., 2001), the most convenient and promising approach to quantitatively investigate the relationship between atmospheric properties and the 3-D canopy light environment is to use a fully coupled atmosphere–canopy radiative transfer model, which enables accurate treatment of multiple scattering between the atmosphere and canopy.

The objective of this study is to describe a 3-D Monte Carlo radiative transfer model (Forest Light Environmental Simulator, FLiES) that can calculate various forest light environmental parameters (canopy reflectance, irradiance at TOC and forest floor, and APAR) including its spatial variation. While 3-D radiative transfer scheme in cloudy atmosphere is one of the potential approaches for the use of our objective, typical spatial scale is quite different between atmosphere (10–1000 km²) and canopy (0.01–1.0 km²) models and computation time is likely to become huge. Therefore we used 1-D radiative transfer scheme in cloudy atmosphere as an initial step.

We emphasize the coupled simulation in atmosphere–vegetation systems to investigate the relationship between the change in atmospheric radiation regime, and APAR and canopy photosynthesis variation in the vegetation canopy. This work is an extension of the calculation conducted by Kobayashi et al. (2007).

2. Model description

Several Monte Carlo canopy radiative transfer models, which are based on different numerical approaches, have been proposed for bidirectional reflectance factor (BRF) calculations. As an extension of the calculation of Kobayashi et al. (2007), we developed a model using the fundamental theory behind Monte Carlo modeling discussed in past studies (e.g., Antyufeev & Marshak, 1990; Iwabuchi, 2006; North, 1996; Ross & Marshak, 1988). We used Antyufeev and Marshak's (1990) method of Monte Carlo photon transport combined with North's (1996) geometric–optical hybrid forest canopy scene. To directly combine the 1-D plane parallel Monte Carlo atmospheric radiative transfer model with the canopy module, we employed the same numerical techniques and sampling methods in both the 1-D atmosphere and the 3-D canopy.

2.1. Simulation scene and optical properties of scattering media

Fig. 1 illustrates the simulation scene, which consists of a plane parallel atmosphere and 3-D vegetation canopy. Table 1 summarizes the atmospheric conditions used in this study. The atmosphere is divided into 12 plane parallel layers, including the height from 0 km (TOC) to 50 km. Each layer has a different density of molecules, aerosols, and cloud particles with different optical properties. We used LOWTRAN-7 (Kneizys et al., 1988) to pre-compute the molecular absorption coefficients under six typical atmospheric profiles, and we used ten aerosol and six cloud types modeled by Hess et al. (1998). Optical properties such as the extinction coefficient for unit volume (β), single scattering albedo (ω), and phase function (p) of each aerosol and cloud type was pre-computed. When we specify the atmospheric profile, aerosol type, and cloud type, the averaged β , ω , and P in the k th atmospheric layer were calculated by averaging the optical properties of all constituents.

$$\beta_{\text{atm},k} = \beta_{\text{m}} + \beta_{\text{a}} + \beta_{\text{c}} \quad (1)$$

$$\omega_{\text{atm},k} = \frac{\omega_{\text{m}}\beta_{\text{m}} + \omega_{\text{a}}\beta_{\text{a}} + \omega_{\text{c}}\beta_{\text{c}}}{\beta_{\text{m}} + \beta_{\text{a}} + \beta_{\text{c}}} \quad (2)$$

$$P_{\text{atm},k} = \frac{\omega_{\text{m}}\beta_{\text{m}}P_{\text{m}} + \omega_{\text{a}}\beta_{\text{a}}P_{\text{a}} + \omega_{\text{c}}\beta_{\text{c}}P_{\text{c}}}{\omega_{\text{m}}\beta_{\text{m}} + \omega_{\text{a}}\beta_{\text{a}} + \omega_{\text{c}}\beta_{\text{c}}} \quad (3)$$

The subscripts atm, m, a, and c indicate the atmosphere, molecular, aerosol, and cloud, respectively.

In the canopy layer, we used a 3-D canopy object scene (Fig. 1). The tree canopy was modeled as a combination of geometric shapes representing the tree crowns (e.g., cones, cylinders and ellipsoids). The stem was modeled as a cylinder and did not enter the tree crown. Instead, the woody matter within the tree crown was modeled as a single object of identical shape, but half the dimensions, located at the lower part of the tree crown. Leaf area density (u) and branch area density (b) within the single canopy and branch media were assumed to be spatially uniform. Understorey vegetation was modeled as a plane parallel layer. In the canopy layer, we assumed that photons interact only with

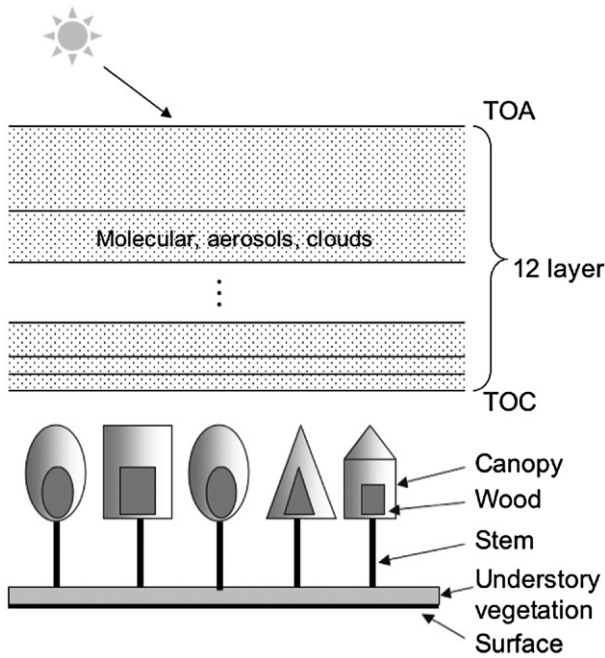


Fig. 1. Schematic illustration of the simulation scene. We used a 1-D plane parallel atmosphere and a 3-D canopy scene.

vegetation media and there are no interactions with atmospheric particles. Optical properties such as the extinction coefficient for unit volume ($\beta_{\text{cnp},k}$), single scattering albedo of a single leaf ($\omega_{\text{cnp},k}$), and phase function ($P_{\text{cnp},k}$) were used as optical properties in the k th canopy object. $\beta_{\text{cnp},k}$ is expressed as a product of the G and leaf area density (u_k):

$$\beta_{\text{cnp},k}(\Omega) = G(\Omega)u_k. \quad (4)$$

The G is the fraction of average projected leaf area along the direction of photon propagation (Ω).

$$G(\Omega) = \frac{1}{2\pi} \int_0^{2\pi} \int_0^{\frac{\pi}{2}} g_L(\Omega_L) |\Omega_L \cdot \Omega| d\Omega_L d\theta_L d\phi_L. \quad (5)$$

The g_L and $\Omega_L(\theta_L, \phi_L)$ are a leaf angle distribution function and a normal vector of the leaf surface, respectively. In our model schemes, any shape of g_L can be potentially used in Eq. (5). The uniform leaf angle distribution was assumed in all

Atmospheric layer (top) km	12 layer	1, 2, 3, 4, 6, 8, 10, 12, 16, 20, 30, 50
Atmospheric profile	6 profile (LOWTRAN-7)	Tropical, mid-latitude summer/winter, high-latitude summer/winter, US standard atmosphere
Aerosol type	10 type (Hess et al., 1998)	Continental (clean, average, polluted), urban, desert, maritime (clean, polluted, tropical), arctic, antarctic
Cloud type	6 type (Hess et al., 1998)	Stratus (continental, maritime), cumulus (continental clean, polluted, maritime), fog

calculation in this study ($G=0.5$). The integration of u_k along the vertical direction is commonly known as leaf area index (LAI). $\omega_{\text{cnp},k}$ is expressed as the sum of single leaf reflectance (r_k) and transmittance (t_k).

$$\omega_{\text{cnp},k} = r_k + t_k. \quad (6)$$

The phase function of the k th canopy component ($P_{\text{cnp},k}$) is expressed as (Shultis & Myneni, 1988):

$$P_{\text{cnp},k}(\Omega', \Omega) = \frac{2}{\omega_{\text{cnp},k}G(\Omega)} \int_{2\pi} g_L(\Omega_L) |\Omega' \cdot \Omega| p_{L,k}(\Omega', \Omega, \Omega_L) d\Omega_L \quad (7)$$

where Ω' and Ω are the photon vector before and after the scattering event, respectively. $p_{L,k}$ is a single leaf phase function for the k th canopy given the normal of the leaf (Ω_L). Scattering within the woody object was also calculated using Eq. (7). In this case we set the transmittance from the woody matter to be zero. Lambertian was assumed for scattering on soil and stem surface.

2.2. Photon tracing and scattering

Figs. 2 and 3 show flowcharts of photon tracing in the atmosphere and the canopy. The model starts the tracing of the

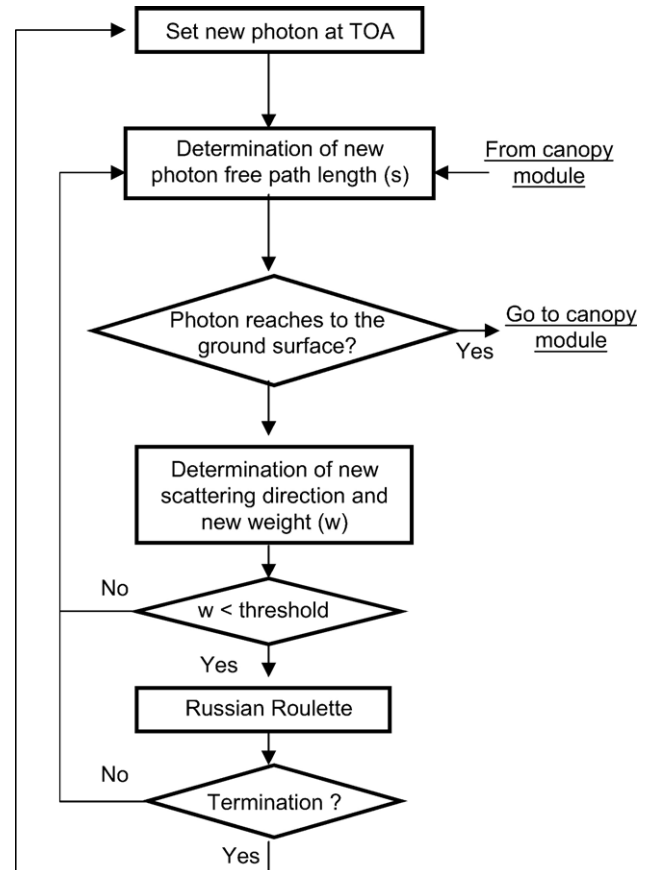


Fig. 2. Flowchart of photon tracing in the atmosphere.

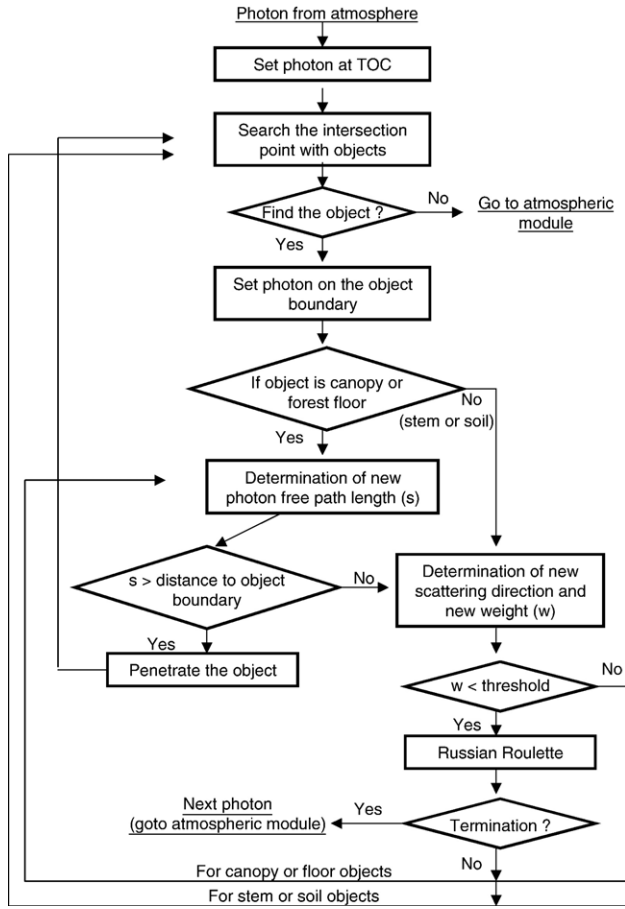


Fig. 3. Flowchart of photon tracing in the canopy.

$\Omega(\theta, \phi)$. Fig. 4 shows an example of the relationship between the random number R and the prescribed scattering angle (α) in the lowest atmospheric layer and in the canopy foliage.

When a periodic condition is assumed for horizontal boundaries, the outgoing photon from the lateral face re-enters from the opposite side of the face with same photon direction and weight. As shown in the flowcharts in Figs. 2 and 3, the weight of photon changes after a scattering. This then enables to easily sample various light environments to this study (BRF, APAR in the canopy and downward radiation) simultaneously. Thus after the j th interaction the weight of a non-absorbed part of photon becomes:

$$w_{j+1} = w_j \omega \tag{10}$$

2.3. Variance reduction technique

2.3.1. Random cut off of the photon

For the reduction of the computation time, the photon with a low weight should be randomly cut off using the “Russian roulette” technique in the model. In the actual simulation, very small weight of photon sometimes remains in the simulation landscape until large and unrealistic order of scattering has been finished. This technique can avoid it and save the computation time. This unbiased technique is widely used in canopy and atmospheric radiative transfer modeling (e.g., Marchuk et al., 1980; Iwabuchi, 2006; Ross & Marshak, 1988). In this technique, when the weight of the photon

photon with initial weight ($w_0=1$) from the top of the atmosphere (TOA). To determine the photon traveling path length (s), optical thickness τ in the atmosphere and the canopy was first determined using a random number (R).

$$\tau = -\ln R. \tag{8}$$

A scattering event should occur at the point, where the optical thickness that is integrated along the photon traveling path is equal to τ in the above equation. The new photon direction $\Omega(\theta, \phi)$ after scattering was determined using the random numbers. When P is dependent only on the scattering angle α ($=\cos^{-1}[\Omega' \cdot \Omega]$) in such cases as atmosphere and canopy with a uniform leaf angle distribution, the α is determined by the look-up-table derived from the following relationship:

$$\frac{1}{2} \int_0^\alpha P(\alpha') \sin \alpha' d\alpha' = R. \tag{9}$$

In this case, the azimuth angle relative to the scattering coordinate ϕ_s was determined randomly. Then the scattering direction $\Omega(\theta, \phi)$ in the cartesian coordinate system was calculated by a coordinate transformation from $\Omega_s(\alpha, \phi_s)$ to

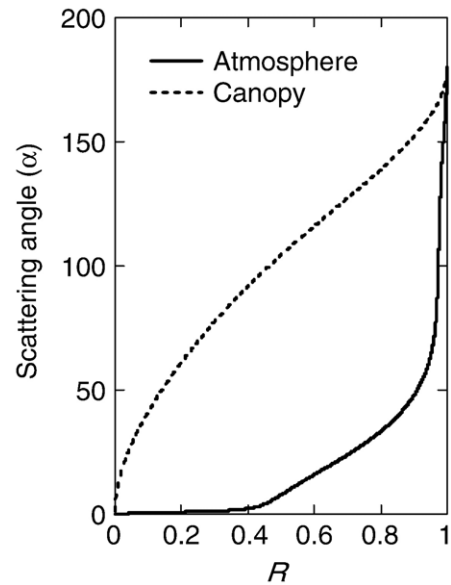


Fig. 4. An example of the relationship between scattering angle (α) and random number (R) in the atmosphere (the lowest layer) and canopy. The function of the atmosphere was calculated for the following conditions. Atmospheric profile: mid-latitude summer, aerosol: desert and optical thickness: 0.3, cloud: stratus continental and optical thickness: 5.0, wavelength=550 nm. The function of the canopy was calculated by the following condition: $\rho^*=0.2$, $\tau^*=0.1$, Uniform leaf angle distribution ($G=0.5$).

becomes smaller than the given threshold (ϵ), the photon is cut off by the given probability ($1-q$). When the photon survives with a probability q , the weight of the photon is modified following w/q so as not to give rise to artificial biases.

In this simulation, we employed the 5% and 10% values of the canopy average $\omega_{\text{cnp},k}$ over all canopy as a threshold (ϵ) and survival probability (q). Under these conditions, “Russian roulette” is applied after approximately third order scattering in visible region ($\omega_{\text{cnp},k} \approx 0.1$) and after less than tenth order scattering in the near infrared region ($\omega_{\text{cnp},k} \approx 0.8$).

2.3.2. Collision-forcing method

When the leaf area density of the canopy and forest floor media is too small, scattering events rarely occur. Because light environmental parameters are sampled at each scattering event, sufficient sampling is not expected in such a small leaf area density case. One of the simple methods to overcome this issue is the collision-forcing method (Iwabuchi, 2006). This method artificially enhances the β_{cnp} to generate a large number of scattering events in the thin media. The single scattering albedo and phase function are adjusted to be invariant before and after the scaling. While the method was originally developed for the atmospheric radiative transfer problem with optically thin media, it is directly applicable for 3-D canopy radiative transfer modeling. And, as described by Iwabuchi (2006), this is an unbiased method. When the leaf area density is small, we can scale the $\beta_{\text{cnp},k}$ to $\beta'_{\text{cnp},k}$ ($\beta_{\text{cnp},k} < \beta'_{\text{cnp},k}$). Then $\omega_{\text{cnp},k}$ and P_{cnp} are also scaled as:

$$\omega'_{\text{cnp},k} = 1 - (1 - \omega_{\text{cnp},k})f_e \quad (11)$$

$$P'_{\text{cnp},k}(\alpha) = 2f_d\delta(\alpha) + (1 - f_d)P_{\text{cnp},k}(\alpha) \quad (12)$$

where f_e is the ratio of the extinction coefficient before and after scaling ($\beta_{\text{cnp},k}/\beta'_{\text{cnp},k}$) and δ is a Dirac delta function. The fraction f_d is expressed as:

$$f_d = \frac{1 - f_e}{\omega'_{\text{cnp},k}} \quad (13)$$

In radiative transfer modeling, when the photon enters the optically thin canopy object, the extinction coefficient is scaled. Then the new direction of the photon and the change in photon weight (Eq. (10)) are determined by $\omega'_{\text{cnp},k}$ and $P'_{\text{cnp},k}$. In the determination of the new direction, the random number (R) is first compared to f_d . If $R < f_d$, the scattering direction is unchanged, whereas if $R > f_d$, the scattering direction is determined by Eq. (9). The BRF and APAR, which are described in the next section, are sampled in every scattering event. In the local estimation of BRF, the second term of the right hand side of Eq. (12) is employed instead of $P_{\text{cnp},k}$.

2.3.3. Truncation approximation

The phase function of aerosols and cloud has strong forward peaks. When such a peaked phase function is used with the local estimation method for BRF calculations described in the next

section, extraordinarily large values are sampled with small probability, resulting in significant noise. To prevent this, we employed the truncation approximation in the atmospheric simulation (Iwabuchi, 2006).

2.4. Sampling of BRF, APAR, and irradiance

Light environmental variables, such as BRF at TOC and TOA, APAR in the canopy, irradiance at the TOC and at the forest floor, and the sunlit leaf area, are major variables for calculating photosynthetic activity and satellite signals. To know the spatial distributions of these variables in the 3-D canopy, pixel- and voxel-based samplings are practical. When each pixel and voxel in the simulated landscape does not overlap each other, total horizontal area A_{tot} and total volume V_{tot} in the simulated landscape can be expressed as:

$$A_{\text{tot}} = \sum_l A(l) \quad (14)$$

$$V_{\text{tot}} = \sum_m V(m). \quad (15)$$

Where $A(l)$ and $V(m)$ are an area in l th pixel and m th volume. In our simulation all variables are sampled with these unit area and volume basis.

BRF at TOC and TOA was sampled using a local estimation method (Antyufeev & Marshak, 1990; Marchuk et al., 1980). This method analytically calculates the contribution for BRF after every scattering. The reflectance contribution factor $\Psi(\Omega_o)$ of the j th scattering event for the direction Ω_o was sampled using the formula:

$$\Psi_j(\Omega_o) = \frac{w_{j+1}P(\Omega_j, \Omega_o)\exp(-\tau')}{4\pi|\cos\theta_o|}. \quad (16)$$

Here P indicates either $P_{\text{atm},k}$ or $P_{\text{cnp},k}$, which depends on the media at scattering point. τ' is a modified optical thickness for the hotspot effect which is the strong backscattering effect near the solar direction ($\Omega_s = -\Omega_o$). To include the hotspot effect in the canopy scattering, we adjusted original optical thickness τ , which is the optical distance from the scattering point (r_{sca}) to a detector at TOC or TOA point (r_{obs}), using some hotspot function (H).

$$\tau' = \tau H(\Omega_j, \Omega_o) \quad (0 \leq H \leq 1). \quad (17)$$

In Eq. (17), various types of hotspot function are available if they are normalized in $[0-1]$. Here we use a simple approximation of the hotspot function proposed by Hapke (1994):

$$H(\Omega_j, \Omega_o) \cong 1 - \frac{1}{\left(1 + \frac{1}{h(\Omega_j, \Omega_o)} \tan(\alpha/2)\right)} \quad (18)$$

where h is expressed as

$$h(\Omega_j, \Omega_o) \cong \frac{u_k l_k}{2} \left(\frac{G(\Omega_j) + G(\Omega_o)}{2} \right) \quad (19)$$

l_k is the radius of the disk-shaped flat leaves.

Table 2
Summary of the simulation conditions

	This study	6S	Streamer
Solar zenith angle and atmospheric profile	Tropical (20°), Mid-latitude summer (40°), High-latitude/Subarctic summer (60°)		
Aerosol type	Continental average ^a	Continental	Rural
	Maritime clean ^a	Maritime	Maritime
AOT	0.0–5.0 (@ 550 nm)	0.0–5.0 (@ 550 nm)	0.0–5.0 (@ 600 nm)
Cloud type	Stratus continental ^a	N/A	Stratus continental ^a
Cloud top height	2 km	N/A	2 km
COT	0.0–20.0 (@ 550 nm)	N/A	0.0–20.0 (@ 600 nm)
Surface type	Lambertian	Lambertian	Lambertian
Surface reflectance	0.1	0.1	0.1
Irradiance/radiance	Both	Irradiance only	Both
Number of stream	–	–	24

AOT: aerosol optical thickness, COT: cloud optical thickness.

^a Hess et al. (1998).

BRF at TOC and TOA of the l th pixel in the simulated landscape is calculated by summing all contributing factors:

$$\text{BRF}(l, \Omega_o) = \frac{\pi}{nA(l)} \sum_{i=1}^N \sum_{j=1}^{M_i} \begin{cases} \Psi_{i,j} & (r_{\text{obs}} \in A(l)) \\ 0 & (r_{\text{obs}} \notin A(l)) \end{cases} \quad (20)$$

where N is the total number of photons. M_i is the number of scattering times for the i th photon, respectively. The n is an incident photon density at TOA [m^{-2}].

$$n = \frac{N}{A_{\text{tot}}} \quad (21)$$

As formulated in the Eq. (20), BRF is only sampled when r_{obs} is located in the pixel $A(l)$. Eqs. (16) and (20) can be also used for calculating the angular variation of downward diffuse radiance incident at TOC. In this case, τ' is an atmospheric optical thickness from the scattering point to TOC, and π in Eq. (20) is replaced by the downward spectral solar flux at TOA (F_{λ} , [$\text{W m}^{-2} \text{nm}^{-1}$ or $\mu\text{mol m}^{-2} \text{s}^{-1} \text{nm}^{-1}$]).

APAR [W m^{-3} or $\mu\text{mol m}^{-3} \text{s}^{-1}$] of the m th voxel can be calculated by simply sampling the change in photon energy in every scattering event occurring within the voxel:

$$\text{APAR}(m) = \frac{F_{\text{par}}}{nV(m)} \sum_{i=1}^N \sum_{j=1}^{M_i} \begin{cases} w_{i,j}(1 - \omega_{\text{cnp},k}) & (r_{\text{sca}} \in V(m)) \\ 0 & (r_{\text{sca}} \notin V(m)) \end{cases}, \quad (22)$$

$$(F_{\text{par}} = \int_{400}^{700} F_{\lambda} d\lambda).$$

As well as Eq. (20), BRF is only sampled when the scattering point r_{sca} is located in the voxel $V(m)$. The APAR of the direct irradiance (APAR_{dir}) can be evaluated by counting only the contribution from the first order scattering ($j=1$), and the APAR of the diffuse irradiance (APAR_{dif}) can be evaluated by

neglecting the contribution from the first order scattering ($j=1$) in Eq. (22).

Downward irradiance of the l th pixel in horizontal plane at height z [m], $I_z(l)$, can be calculated by counting the photon weight that passes through the horizontal plane.

$$I_z(l) = \frac{F_{\lambda}}{nA(l)} \sum_{i=1}^N \sum_{j=1}^{M_i} \begin{cases} w_{i,j} & (r_z \in A(l)) \\ 0 & (r_z \notin A(l)) \end{cases} \quad (23)$$

As well as Eqs. (20) and (22), the irradiance is only sampled when the point r_z is located in the pixel with $A(l)$. As in the case in APAR_{dif} sampling, the direct and diffuse irradiances can be separately evaluated.

The sunlit leaf area density in a unit voxel (u_s [m^{-1}]) can be calculated by counting the number of photons from the first scattering.

$$u_s = \frac{1}{G(\Omega_{j=0})nV(m)} \sum_{i=1}^N \begin{cases} 1 & (r_{\text{sca}} \in V(m)) \\ 0 & (r_{\text{sca}} \notin V(m)) \end{cases} \quad (24)$$

In Eq. (24), weight is sampled only if the first scattering occurs in the voxel.

2.5. Spectral integration in PAR and shortwave

Light environmental variables described in Section 2.4 are calculated by integrating variables over a spectral region, such as PAR, and shortwave spectral ranges. The number of photon in each waveband ($\Delta\lambda$) needs to be determined by the weight which is proportional to F_{λ} . When N photons are used for the

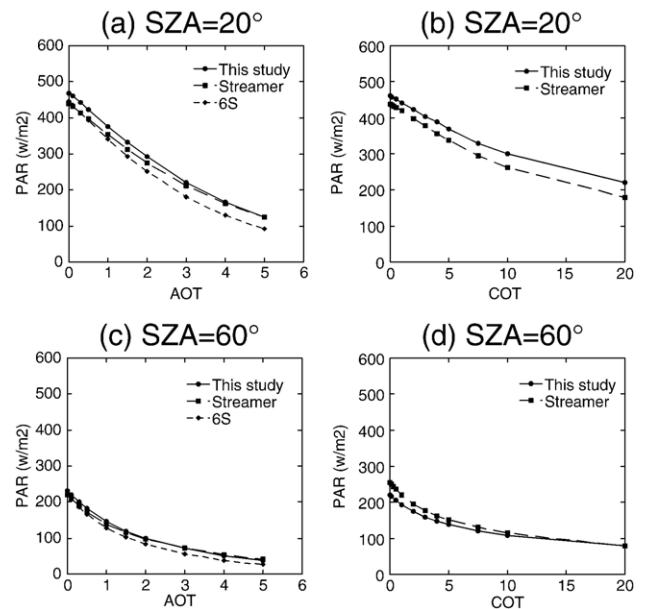


Fig. 5. Simulated downward PAR at TOC from our model, Streamer, and 6S. (a) Clear sky case: SZA=20, tropical atmosphere, and continental aerosol, (b) Cloudy sky: SZA=20, tropical atmosphere, and AOT=0.1, (c) Clear sky case: SZA=60, high-latitude atmosphere, and continental aerosol, (d) Cloudy sky: SZA=60, high-latitude atmosphere, and AOT=0.1.

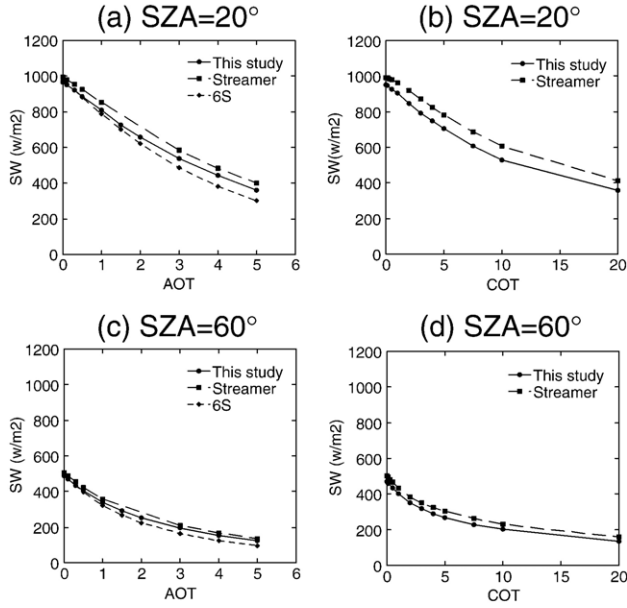


Fig. 6. Simulated downward SW at TOC from our model, Streamer, and 6S. (a) Clear sky case: SZA=20, tropical atmosphere, and continental aerosol, (b) Cloudy sky: SZA=20, tropical atmosphere, and AOT=0.1, (c) Clear sky case: SZA=60, high-latitude atmosphere, and continental aerosol, (d) Cloudy sky: SZA=60, high-latitude atmosphere, and AOT=0.1.

radiative transfer calculation in the spectral ranges $[\lambda_{\min}, \lambda_{\max}]$, the number of photons (N_i) in the i th waveband $[\lambda_i, \lambda_{i+1}]$ is:

$$N_i = N \frac{\int_{\lambda_i}^{\lambda_{i+1}} F_\lambda d\lambda}{\int_{\lambda_{\min}}^{\lambda_{\max}} F_\lambda d\lambda}, \quad \left(\sum N_i = N \right). \quad (25)$$

In this case, the weight and energy of the single photon are the same in all spectral calculations.

2.6. Canopy photosynthesis simulation

The light environmental variables calculated from the radiative transfer simulation can be directly used for canopy photosynthesis simulation. We simulated canopy photosynthesis based on Farquhar's leaf photosynthesis model (Farquhar et al., 1980).

In the calculation, we ignored the spatial heterogeneity of the light environment within a single voxel to simplify the calculation. Two representative leaves (sunlit leaf and shaded

leaf) were then used for the single voxel photosynthesis calculation. Diffuse light was assumed to be incident from the upper hemispherical direction, because diffuse PAR contribution from downward hemisphere is small. Under these assumptions, photosynthesis in a single voxel (PSN(m)) can be expressed as a summation of photosynthesis rate from sunlit and shaded leaves:

$$\begin{aligned} \text{PSN}(m) = & \frac{u_s}{2\pi} \int_{2\pi} \text{PSN}_{\text{leaf}}(\text{APAR}_{\text{leaf,sun}}) g_L(\Omega_L) d\Omega_L \\ & + \frac{(u - u_s)}{2\pi} \int_{2\pi} \text{PSN}_{\text{leaf}}(\text{APAR}_{\text{leaf,shade}}) g_L(\Omega_L) d\Omega_L \end{aligned} \quad (26)$$

where PSN_{leaf} is a leaf photosynthesis rate and $\text{APAR}_{\text{leaf,sun}}$ and $\text{APAR}_{\text{leaf,shade}}$ are the APAR in the unit leaf area $[\mu\text{mol m}^{-2} \text{s}^{-1}]$ for sunlit and shaded leaves, respectively.

$$\text{APAR}_{\text{leaf,sun}} = I_{\text{dir,TOC}} \times |\Omega_s \cdot \Omega_L| \times (1 - \omega_{\text{cnp},k}) + \frac{\text{APAR}_{\text{dif}}}{u} \quad (27)$$

$$\text{APAR}_{\text{leaf,shade}} = \frac{\text{APAR}_{\text{dif}}}{u} \quad (28)$$

where $I_{\text{dir,TOC}}$ $[\text{W m}^{-2}]$ is downward irradiance at TOC calculated by the equation similar to Eq. (23). It should be noted that Eq. (26) does not distinguish the adaxial and abaxial

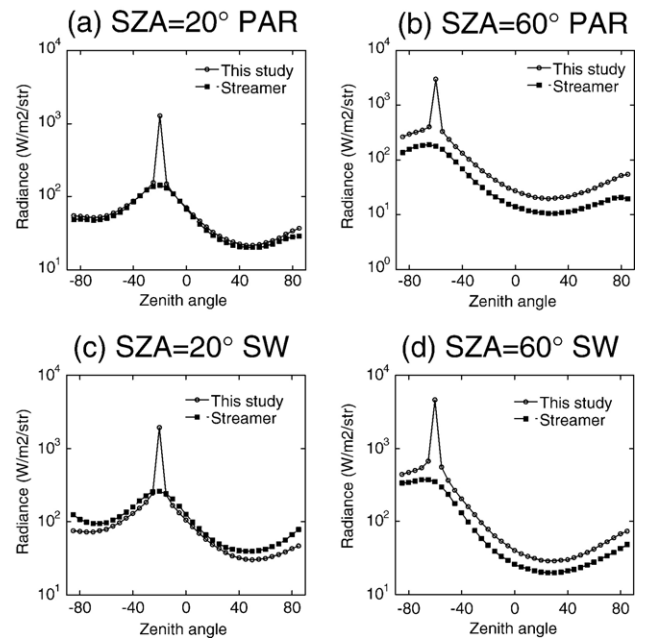


Fig. 7. Comparison of the downward diffuse PAR and SW radiance at TOC. (a) and (c) Clear sky case: SZA=20, and tropical atmosphere, (b) and (d) Clear sky case: SZA=60, high-latitude atmosphere, and continental aerosol. The negative angle indicates the solar direction.

Table 3
Root mean square differences

	This study—6S (Clear sky)	This study—Streamer (Clear sky)	This study—Streamer (Cloudy sky)
RMS difference (PAR)	28.7	33.8	36.5
RMS difference (SW)	24.6	24.9	51.5

(Unit: W m^{-2}).

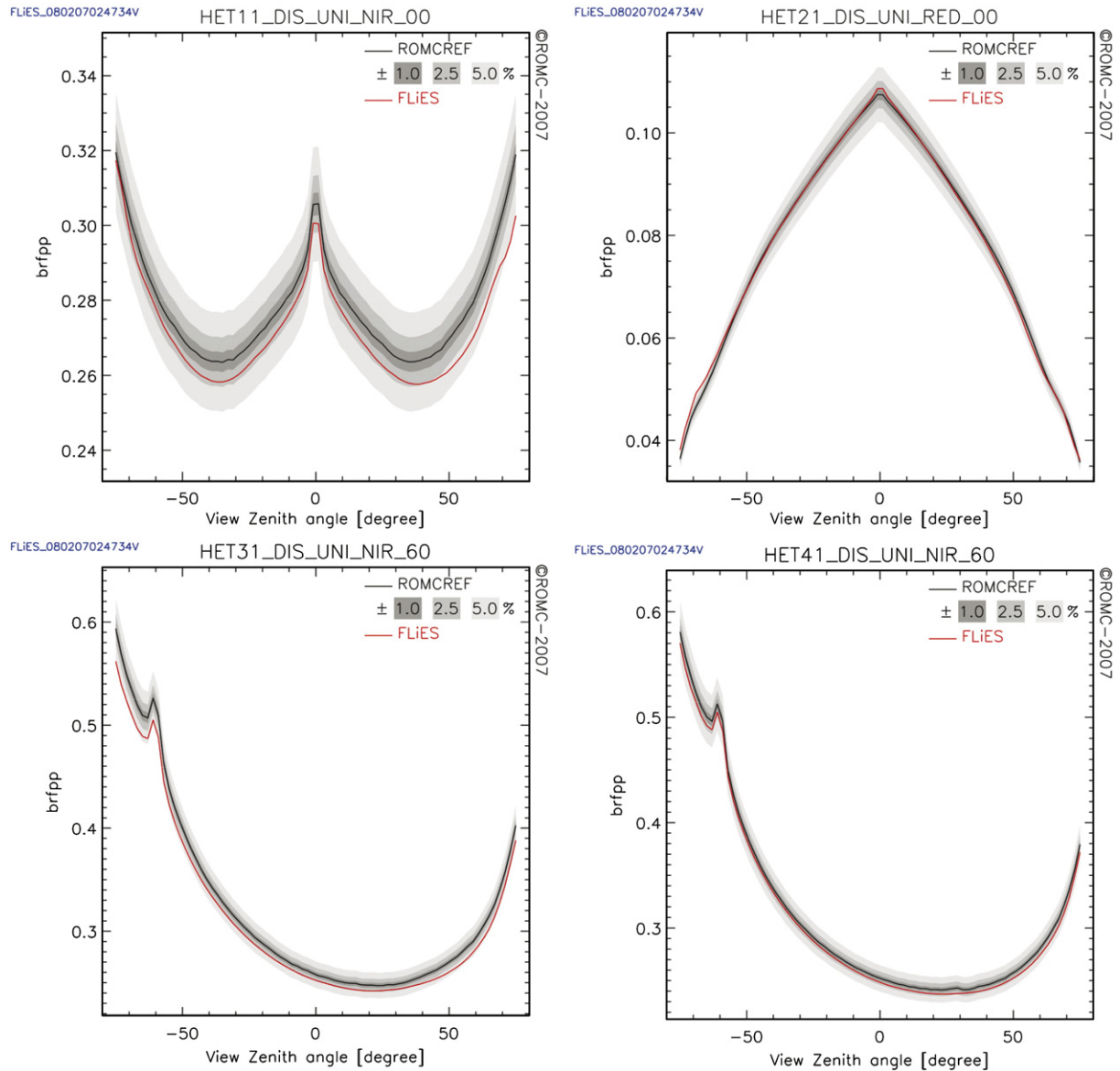


Fig. 8. Graphs generated by the RAMI On-line Model Checker showing BRF simulations of our model (FLiES) and the reference data (ROMCREF) for four heterogeneous canopy scenarios covering an area of 1 ha. Shown are BRF simulations for the principal plane (brfpp) in both the red and the near-infrared (NIR) spectral domain for direct illumination conditions with a zenith angle of 0° (top panels) and 60° (bottom panels).

side of the leaf. Thus both sides of the leaf are assumed to have the same photosynthetic ability.

3. Comparison to other models

3.1. Atmospheric module

Comparisons between our model and other 1-D atmospheric radiative transfer models are helpful to understand differences in the atmospheric module. We selected two widely used models for the comparison study: Second Simulation of the Satellite Signal in the Solar Spectrum (6S, Vermote et al., 1997), and Streamer version 3.0 (Key & Schweiger, 1998; Key, 2001). Both models can simulate the irradiance in the solar spectral domain SW (0.3–4.0 μm) and have similar pre-defined atmospheric, aerosol, and

cloud type conditions. Table 2 summarizes the atmospheric conditions used in the comparisons. Although we compared the simulation results in similar aerosol and cloud types, optical properties in these types are not exactly the same.

We calculated the downward irradiance and radiance at TOC averaged over PAR (0.4–0.7 μm) and SW (0.3–4.0 μm). PAR calculated by Streamer uses slightly different spectral ranges (0.4–0.69 μm), because this model calculates the irradiance and radiance on a spectral band basis (Band 120–Band 125). The 6S uses only an irradiance simulation under clear sky.

Figs. 5 and 6 show the result examples of the incident PAR and SW at TOC in tropical and high-latitude summer. The root mean square (RMS) differences for all simulation cases (Table 3) ranged from 24.6 to 51.5 (W m^{-2}). Aerosol optical thickness (AOT) and cloud optical thickness (COT) dependency of our

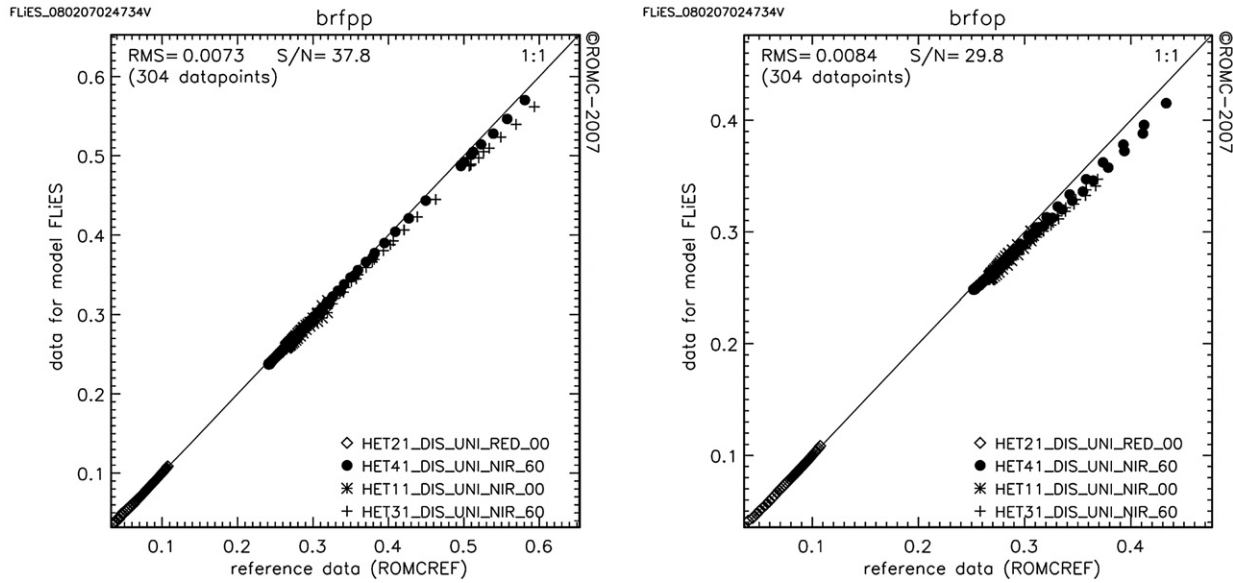


Fig. 9. ROMC generated graph of the BRF simulations of our model (FLiES) and the reference data (ROMCREf). The left panel refers to BRF simulations in the principal plane that were shown in Fig. 8, the right panel refers to simulations in the orthogonal plane. Indicated are also the root mean square error (RMS) and the signal to noise ratio (S/N).

model showed reasonable agreement with other models. Most of the differences among models were bias differences, especially in tropical atmosphere cases. Since these differences exist even in very low AOT and COT conditions, possible sources of the differences could be the slightly different PAR spectral coverage in Streamer and the difference of absorption coefficients in pre-defined atmospheric profiles.

Fig. 7 shows comparisons of the downward PAR and SW radiance at TOC along the principal plane. The directionality of the radiance follows almost the same course except around the solar

direction. Our model can express the strong radiance peak near the solar direction due to sharp forward scattering by aerosol particles.

3.2. Comparison to RAMI results

The Radiation transfer Model Intercomparison (RAMI) activity is an open-access community driven benchmarking effort to evaluate the accuracy and reliability of canopy radiation transfer models (Pinty et al., 2001, 2004, Widlowski et al., 2007). During the third phase of RAMI the mutual agreement amid six different 3-D Monte Carlo models lay for the first time within 1% of each other which prompted the establishment of a so-called “surrogate truth” dataset against which other models may now be compared. To facilitate this task an automated web-based tool called the RAMI On-line Model Checker (ROMC) was made available at <http://romc.jrc.it/> (Widlowski et al., 2007). The ROMC allows both the

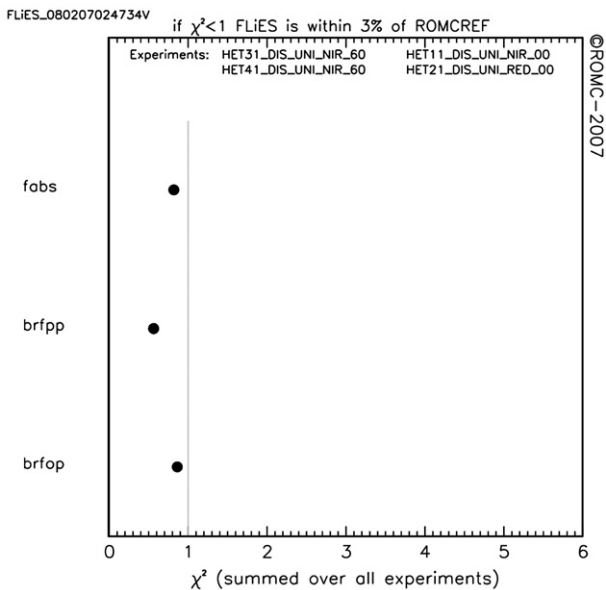


Fig. 10. ROMC generated graph of the overall model discernability (χ^2) between our model (FLiES) and the reference data (ROMCREf).

Table 4
Parameters used in the simulation

Atmosphere	
Solar zenith angle	40°
Atmospheric profile	Mid-latitude summer
Aerosol type	Continental average
AOT	0.0, 0.1, 0.3, 0.5, 1.0, 2.0, 3.0, 4.0, 5.0
Canopy	
Leaf reflectance/transmittance	0.0546/0.0149 (Red) 0.4957/0.4409 (NIR) 0.1/0.05 (PAR)
Surface reflectance	
	0.127 (Red) 0.159 (NIR) 0.1 for soil, 0.8 for snow (PAR)
Landscape-averaged LAI	
	0.5, 2.5, 5.0

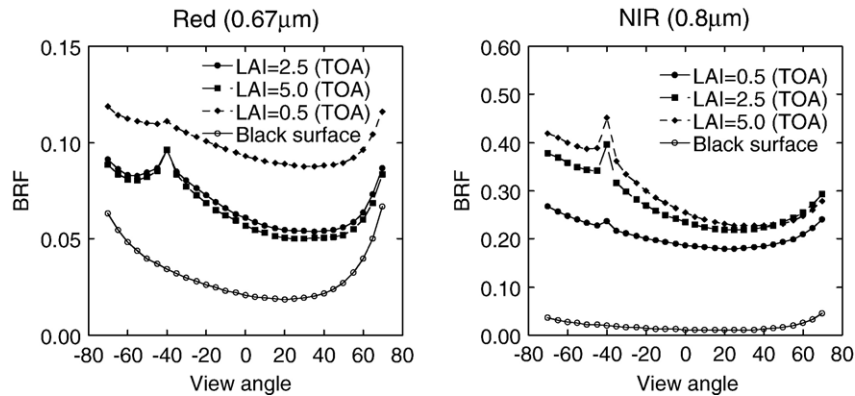


Fig. 11. Angular variations in bidirectional reflectance factor (BRF) at TOC and TOA on the solar principal plane (AOT=0.1).

comparison of model simulations against already published RAMI results (debug mode), and, the ‘blind’ evaluation of models against a small set of randomly drawn test cases whose results cannot be known a priori (validate mode). We used four different heterogeneous canopy landscapes in its ‘Validation mode’. Also, in this experiment, we did not use the atmospheric module and input the photon from TOC directly.

Figs. 8, 9 and 10 were generated by the ROMC and certify the performance of the model in validate mode. Fig. 8 shows the angular variability of BRF on the principal plane. The simulated results in the red spectral region (HET21_DIS_UNL_RED_00) agreed well with ROMC reference dataset (ROMCREF), including around the hotspot shapes, despite the use of the simple hotspot function in our model. Although the results in NIR were slightly smaller than ROMCREF, especially in HET11_DIS_UNL_NIR_00, the absolute differences were less than 0.01 (Figs. 8 and 9). The RMS differences between our model and ROMCREF were 0.0073 for the principal plane and 0.0084 for the orthogonal plane, respectively. Fig. 10 shows the model discernability (χ^2) (Pinty et al., 2001) in the BRF on the principal and orthogonal planes, and absorbed radiation in the canopy (fabs). The χ^2 of both the BRF and the fabs simulation results were smaller than unity, indicating that the simulations of FLIES were not discernable (to within 3%) from those of the ROMCREF dataset. Overall the ROMC results in validate mode (4 test cases) suggest that our model yields results that are similar to those of state-of-the-art 3-D Monte Carlo models both for total BRF and canopy absorption estimates.

4. Application of the model for light environmental simulation

4.1. Simulation conditions

The same canopy sizes and positions as ‘floating spheres’ experiment of RAMI (Pinty et al., 2001) was employed as a testing canopy landscape to investigate the mutual dependency of both atmospheric and terrestrial radiative properties under a variety of spectral, structural and optical thickness conditions. The various atmospheric and canopy conditions are summarized in Table 4. Leaf reflectance/transmittance and soil reflectance in red and near

infrared (NIR) were the same values as defined in the ‘floating sphere’ scene in RAMI. Although APAR simulation requires the spectral information of canopy/surface optical properties for spectral integration (Section 2.5), we used spectrally constant optical properties for the simplicity in this simulation.

In Pinty et al. (2001), LAI was defined as an individual sphere value, instead of landscape-averaged value. We defined LAI as a landscape-averaged one (100×100 m) and three different landscape-averaged LAI (LAI=0.5, 2.5 5.0) was used. And woody dominant regions in sphere canopies defined in our model (Section 2.1), which are not defined in the original ‘floating sphere’ landscape, were assumed to be empty (no woody material). Canopy photosynthesis was also calculated using the formulae in Section 2.6, and the same biochemical parameters as summarized by De Pury and Farquhar (1997) were employed.

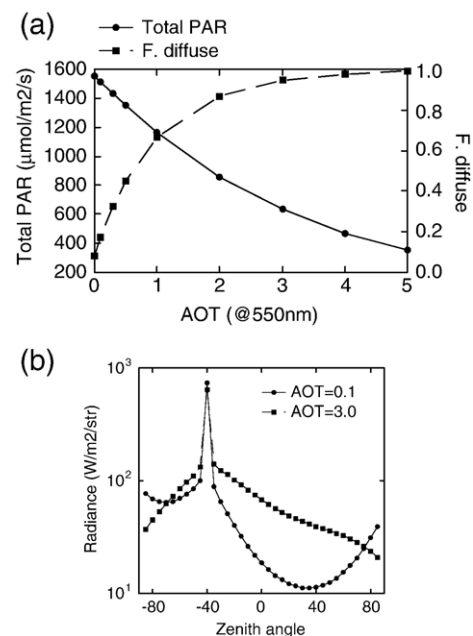


Fig. 12. (a) Downward total PAR and fraction of diffuse PAR (F. diffuse) at TOC as a function of AOT. (b) Diffuse PAR radiance as a function of incident angle (zenith angle) at TOC along the solar principal plane. The negative angle indicates the solar direction. Atmospheric conditions: Clear day, SZA=40, Mid-latitude summer, Continental average aerosol.

4.2. Application results

Scene-averaged BRFs at TOA in three LAI cases and black surface (surface reflectance=0.0) case are shown in Fig. 11. The atmospheric scattering contribution for BRF can be quantified by comparing with BRF in black surface condition. The atmospheric effect on BRF (40.2% in nadir view and LAI=5.0) in red is larger than that in NIR (11.2% in nadir view and LAI=5.0). In these BRF, the reflectance contribution from the canopy (10.8%) in red is much smaller than that from the forest floor (49.0%). In contrast, the NIR reflectance contribution from the canopy (71.2%) is much higher than that from the forest floor (17.6%).

The simulated downward PAR irradiance and radiance directionality at TOC are shown in Fig. 12. PAR irradiance

decreases as AOT increases and the fraction of diffuse PAR drastically increases at $AOT < 1.0$ (Fig. 12(a)). The angular distribution of downward PAR radiance depends highly on the AOT. In thin aerosol conditions ($AOT=0.1$), diffuse radiance peaks near the solar direction due to the strong forward scattering properties of aerosol particles. Although directionality in diffuse PAR radiance becomes smoother with increasing AOT, diffuse PAR at $AOT=3.0$ still retains directionality (Fig. 12(b)).

Directionality in PAR directly affects the 3-D APAR distribution in the canopy. Fig. 13 shows the total (direct+diffuse) APAR variations in the canopy along the vertical slice in the center of “floating sphere” landscape. Two AOT ($AOT=0.1$, and 3.0) and three LAI (LAI=0.5, 2.5, 5.0) conditions are displayed (Fig. 13 (a)). Under clear sky conditions ($AOT=0.1$), strong absorption of total APAR occurs in the solar side in each canopy. Under thick

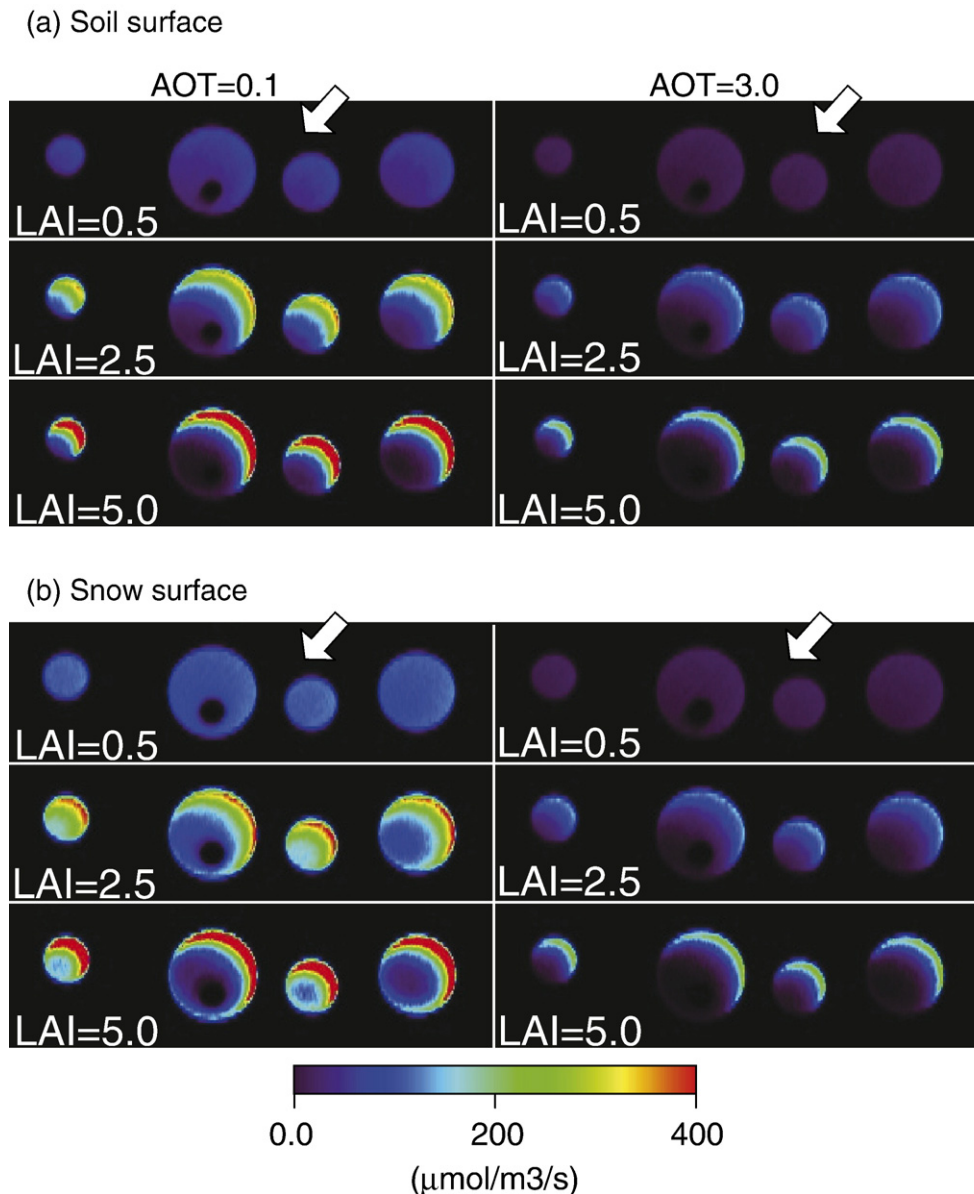


Fig. 13. Vertical slices of the 3-D distribution of total APAR in the “floating sphere” landscape. (a) Soil surface (surface reflectance=0.1), (b) snow surface (surface reflectance=0.8). The solar zenith angle is 40° as indicated by the white arrows.

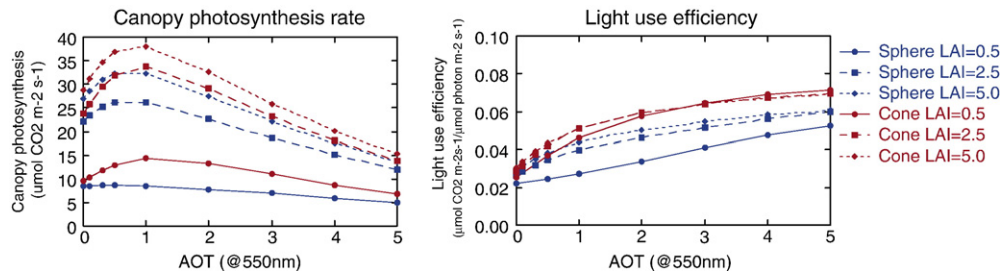


Fig. 14. Canopy photosynthesis rate (left) and light use efficiency (right) as a function of AOT in three LAI and two canopy shape (sphere and cone) cases.

aerosol conditions (AOT=3.0), while over 90% of downward PAR is diffuse (Fig. 12), total APAR is not isotropic but remains strong near the solar side due to the directionality of the downward PAR (Fig. 12(b)). This effect is larger under higher LAI conditions.

The comparison with the APAR distribution under snow surface condition shows the relation of APAR distribution to surface condition (Fig. 13(b)). Under high surface reflective conditions, APAR is enhanced especially around the lower side of canopy due to the effect of reflected radiation from snow surface. Strong enhancements are found in AOT=0.1 case. The landscape-averaged fraction of APAR (fAPAR) in snow surface and LAI=5.0 case is 0.772 and it is 26% higher than soil surface cases (0.612). Although AOT=3.0 case in Fig. 13 does not show the clear contrast between soil and snow surface because incident PAR at TOC is low (Fig. 12), fAPAR in snow surface and LAI=5.0 case (0.789) is 24% higher than soil surface case (0.637). These simulation results indicate that the 3-D distribution of APAR and its fraction to incident radiation depends on surface reflectance.

Fig. 14 (left) shows the canopy photosynthesis in the simulated scene as a function of AOT. In addition to the simulation in original “floating sphere” landscape, we also simulated the cone-shaped canopy landscape. In cone canopy simulation, we used same canopy position and volumes with same landscape-averaged LAI and projected areas from nadir view. All simulated canopy photosynthesis cases show the similar AOT dependency. It initially increases with increasing AOT and then decreases, as has been suggested in past researches (e.g., Cohan et al., 2002).

Canopy shape affects the magnitude of canopy photosynthesis. Photosynthesis in cone-shaped canopy case is higher than that in sphere canopy case. This is mainly due to the difference of the area that is faced on the solar direction. The canopy with larger projected area for solar direction can perform more photosynthesis. Fig. 14 (right) shows the AOT dependency of the light use efficiency (LUE). LUE gradually increase with increase in AOT. However its slope and absolute values depends on the canopy structure and LAI. In cone canopy cases, LUE has similar patterns in three different LAI cases. In contrast, LUE in sphere canopy cases is quite different. This simulation suggests that LAI is not the only parameter to determine the photosynthesis in heterogeneous landscape. For detail understanding of forest canopy photosynthesis, both angular geometry of incident PAR at TOC and 3-D canopy structure should be examined.

5. Conclusion

We described the radiative transfer model in the 1-D atmosphere and 3-D canopy system. For the realistic simulation of the light environment in the canopy, 3-D canopy radiative transfer simulation directly coupled with atmospheric radiative transfer is required. Coupled simulation helps in understanding of the realistic light environment and canopy photosynthesis under various atmospheric conditions and various canopy structures. In this paper, we showed several simulation results as an example. The BRDF simulation at TOA would be useful to evaluate the atmospheric effect on BRDF as well as the effect of 3-D canopy structure. Also the simulation results showed difference in 3-D distributions of APAR in canopy under various atmospheric, canopy, and surface conditions. Even if thick aerosol conditions such as AOT=3.0, total APAR is not isotropic but remains strong near the solar side due to the directionality of the downward PAR. Finally the effect of atmospheric condition and canopy structure on canopy photosynthesis was investigated. For detail understanding of forest canopy reflectance, light environment, and canopy photosynthesis, angular geometry of incident light at TOC and 3-D canopy structure should be considered.

Acknowledgements

We thank Dr. Jean-Luc Widlowski for his helpful handling of the comparison with RAMI-3 data on the ROMC system. Thanks also to Dr. Keiichi Asada for the helpful discussion of the radiative transfer theory. The research was supported by the Japan Society for the Promotion of Science, “KAKENHI Young Scientist B (18710020)”.

References

- Alton, P. B., North, P., Kaduk, J., & Los, S. (2005). Radiative transfer modeling of direct and diffuse sunlight in a Siberian pine forest. *Journal of Geophysical Research*, 110, D23209. doi:10.1029/2005JD006060
- Antyufeev, V. S., & Marshak, A. L. (1990). Monte Carlo method and transport equation in plant canopies. *Remote Sensing of Environment*, 31, 183–191.
- Chameides, W. L., Yu, H., Liu, S. C., Bergin, M., Zhou, X., Mearns, L., et al. (1999). Case study of the effects of atmospheric aerosols and regional haze on agriculture: An opportunity to enhance crop yields in China through emission controls? *Proceedings of the National Academy of Sciences of the United States of America*, 96, 13626–13633.
- Cohan, D. S., Xu, J., Greenwald, R., Bergin, M. H., & Chameides, W. L. (2002). Impact of atmospheric aerosol light scattering and absorption on terrestrial

- net primary production. *Global Biogeochemical Cycles*, 16(4), 1090. doi:10.1029/2001GB001441
- De Pury, D. G. G., & Farquhar, G. D. (1997). Simple scaling of photosynthesis from leaves to canopies without the errors of big-leaf models. *Plant, Cell and Environment*, 20, 537–557.
- Dye, D. G. (2004). Spectral composition and quanta-to-energy ratio of diffuse photosynthetically active radiation under diverse cloud conditions. *Journal of Geophysical Research*, 109, D10203. doi:10.1029/2003JD004251
- Eck, T. F., & Dye, D. G. (1991). Satellite estimation of incident photosynthetically active radiation using ultraviolet reflectance. *Remote Sensing of Environment*, 38, 135–146.
- Farquhar, G. D., von Caemmerer, S., & Berry, J. A. (1980). A biochemical model of photosynthetic CO₂ assimilation in leaves of C3 species. *Planta*, 149, 78–90.
- Frouin, R., Lingner, D. W., Gautier, C., Baker, K. S., & Smith, R. C. (1989). A simple analytical formula to compute clear sky total and photosynthetically available solar irradiance at the ocean surface. *Journal of Geophysical Research*, 94(C7), 9731–9742.
- Gastellu-Etchegorry, J. P., Demarres, V., Pinel, V., & Zagolski, F. (1996). Modeling radiative transfer in heterogeneous 3-D vegetation canopies. *Remote Sensing of Environment*, 58, 131–156.
- Govaerts, Y. M., & Verstraete, M. M. (1998). Raytran: A Monte Carlo ray-tracing model to compute light scattering in three-dimensional heterogeneous media. *IEEE Transactions on Geoscience and Remote Sensing*, 36(2), 493–505.
- Grant, R. H. (1985). The influence of the sky radiance distribution on the flux density in the shadow of a tree crown. *Agricultural and Forest Meteorology*, 35, 59–70.
- Gu, L., Baldocchi, D. G., Wofsy, S. C., Munger, J. W., Michalsky, J. J., Urbansky, S. P., et al. (2003). Response of a deciduous forest to the Mount Pinatubo eruption: Enhanced photosynthesis. *Science*, 299(5615), 2035–2038.
- Gu, J., Smith, E. A., Cooper, H. J., Grose, A., Liu, G., Merritt, J. D., et al. (2004). Modeling carbon sequestration over the large-scale Amazon basin, aided satellite observation part I: Wet- and dry-season surface radiation budget flux and precipitation variability based on GOES retrievals. *Journal of Applied Meteorology*, 43, 870–886.
- Guillevic, P., & Gastellu-Etchegorry, J. P. (1999). Modeling BRDF and radiation regime of boreal and tropical forest: II. PAR regime. *Remote Sensing of Environment*, 68, 317–340.
- Hapke, B. (1994). *Theory of reflectance and emittance spectroscopy*: Cambridge University Press 455 pp.
- Hess, M., Koepke, P., & Schult, I. (1998). Optical properties of aerosols and clouds: The software package OPAC. *Bulletin of the American Meteorological Society*, 79, 831–844.
- Iwabuchi, H. (2006). Efficient Monte Carlo methods for radiative transfer modeling. *Journal of the Atmospheric Sciences*, 63, 2324–2339.
- Key, J. (2001). *Streamer user's guide*, cooperative institute for meteorological satellite studies.: University of Wisconsin 96 pp.
- Key, J., & Schweiger, A. J. (1998). Tools for atmospheric radiative transfer: Streamer and FluxNet. *Computers & Geosciences*, 24(5), 443–451.
- Kneizys, F. X., Shettle, E. P., Abreu, L. W., Chetwynd, J. H., Anderson, G. P., Gallery, W. O., et al. (1988). *User's guide to LOWTRAN 7*. AFGL-TR-88-0177. 137 pp.
- Kobayashi, H., Matsunaga, T., & Hoyano, A. (2005). Net primary production in Southeast Asia following a large reduction in photosynthetically active radiation owing to smoke. *Geophysical Research Letters*, 32, L02403. doi:10.1029/2004GL021704
- Kobayashi, H., Matsunaga, T., Hoyano, A., Aoki, M., Komori, D., & Boonyawat, S. (2004). Satellite estimation of photosynthetically active radiation in Southeast Asia: Impacts of smoke and cloud cover. *Journal of Geophysical Research*, 109, D04102. doi:10.1029/2003JD003807
- Kobayashi, H., Suzuki, R., & Kobayashi, S. (2007). Reflectance seasonality and its relation to the canopy leaf area index in an eastern Siberian larch forest: Multi-satellite data and radiative transfer analyses. *Remote Sensing of Environment*, 106, 238–252.
- Liang, S., Zheng, T., Liu, R., Fang, H., Tsay, S. -C., & Running, S. (2006). Estimation of incident photosynthetically active radiation from Moderate Resolution Imaging Spectrometer data. *Journal of Geophysical Research*, 111, D15208. doi:10.1029/2005JD006730
- Marchuk, G., Mikhailov, G., Nazaraev, M., Darbinjan, R., Kargin, B., & Elepov, B. (1980). *The Monte Carlo methods in atmospheric optics*: Springer-Verlag 208 pp.
- Min, Q. (2005). Impacts of aerosols and clouds on forest-atmosphere carbon exchange. *Journal of Geophysical Research*, 110, D06203. doi:10.1029/2004JD004858
- Myneni, R. B., Marshak, A., Knyazikhin, Y., & Asrar, G. (1991). Discrete ordinates method for photon transport in leaf canopies. In R. B. Myneni, & J. Ross (Eds.), *Photon-vegetation interactions: Applications in optical remote sensing and plant physiology* (pp. 45–109). : Springer-Verlag.
- Nemani, R. R., Keeling, C. D., Hashimoto, H., Jolly, W. M., Piper, S. C., Tucker, C. J., et al. (2003). Climate-driven increases in global terrestrial net primary production from 1982 to 1999. *Science*, 300, 1560–1563.
- Niyogi, D., Chang, H. I., Saxena, V. K., Holt, T., Alapaty, K., Booker, F., et al. (2004). Direct observations of the effects of aerosol loading on net ecosystem CO₂ exchanges over different landscapes. *Geophysical Research Letters*, 31, L20506. doi:10.1029/2004GL020915
- North, P. R. (1996). Three-dimensional forest light interaction model using a Monte Carlo method. *IEEE Transactions on Geoscience and Remote Sensing*, 34(4), 946–956.
- Pinker, R. T., & Laszlo, I. (1992). Modeling surface solar irradiance for satellite applications on a global scale. *Journal of Applied Meteorology*, 31, 194–211.
- Pinty, B., Gobron, N., Widlowski, J. -L., Gerstl, S., Verstraete, M., Antunes, M., et al. (2001). Radiation transfer model intercomparison (RAMI) exercise. *Journal of Geophysical Research*, 106(D11), 11937–11956.
- Pinty, B., Widlowski, J. -L., Taberner, M., Gobron, N., Verstraete, M., Disney, M., et al. (2004). Radiation transfer model intercomparison (RAMI) exercise: Results from the second phase. *Journal of Geophysical Research*, 107, D06210. doi:10.1029/2003JD004252
- Roderick, M. L., Farquhar, G. D., Berry, S. L., & Noble, I. R. (2001). On the direct effect of clouds and atmospheric particles on the productivity and structure of vegetation. *Oecologia*, 129, 21–30.
- Ross, J. K., & Marshak, A. L. (1988). Calculation of canopy bidirectional reflectance using the Monte Carlo method. *Remote Sensing of Environment*, 24, 213–225.
- Sellers, P. J. (1985). Canopy reflectance, photosynthesis and transpiration. *International Journal of Remote Sensing*, 6(8), 1335–1372.
- Sellers, P. J. (1987). Canopy reflectance, photosynthesis, and transpiration. II. The role of biophysics in the linearity of their interdependence. *Remote Sensing of Environment*, 21, 143–183.
- Sellers, P. J., Berry, J. A., Collatz, G. J., Field, C. B., & Hall, F. G. (1992). Canopy reflectance, photosynthesis and transpiration. III. A reanalysis using improved leaf models and a new canopy integration scheme. *Remote Sensing of Environment*, 42, 187–216.
- Shultis, J. K., & Myneni, R. B. (1988). Radiative transfer in vegetation canopies with anisotropic scattering. *Journal of Quantitative Spectroscopy and Radiative Transfer*, 39(2), 115–129.
- Van Laake, P. E., & Sanchez-Azofeifa, G. A. (2004). Simplified atmospheric radiative transfer modeling for estimating incident PAR using MODIS atmosphere products. *Remote Sensing of Environment*, 91, 98–113.
- Vermote, E., Tanre, D., Deuze, J. L., Herman, M., & Morcrette, J. J. (1997). Second simulation of the satellite signal in the solar spectrum, 6S: An overview. *IEEE Transactions on Geoscience and Remote Sensing*, 35(3), 675–686.
- Wang, Y. P., & Jarvis, P. G. (1990). Influence of crown structural properties on PAR absorption, photosynthesis, and transpiration in Sitka spruce: Application of a model (MAESTRO). *Tree Physiology*, 7, 297–316.
- Widlowski, J.-L., Pinty, B., Gobron, N., & Verstraete, M. M. (2001). Detection and characterization of boreal coniferous forests from remote sensing data. *Journal of Geophysical Research*, 106(D24), 33405–33419.
- Widlowski, J., Pinty, B., Laverigne, T., Verstraete, M. M., & Gobron, N. (2006). Horizontal radiation transport in 3-D forest canopies at multiple spatial resolutions: Simulated impact on canopy absorption. *Remote Sensing of Environment*, 103, 379–397.
- Widlowski, J.-L., Taberner, M., Pinty, B., Bruniquel-Pinel, V., Disney, M., Fernandes, R., et al. (2007). The third RADIATION transfer Model Intercomparison (RAMI) exercise: Documenting progress in canopy reflectance modeling. *Journal of Geophysical Research*, 112, D09111. doi:10.1029/2006JD007821